APAM: Antagonistic Pneumatic Artificial Muscle

Nathan S. Usevitch¹, Allison M. Okamura¹, and Elliot W. Hawkes²

Abstract—We present a pneumatic actuator capable of changing length by 1000%, applying both pushing and pulling forces, and independently modulating its length and stiffness. These characteristics are enabled by individually addressable internal and external chambers that work antagonistically against one another. The high deformation with low hysteresis is achieved by wrinkling of thin materials that are assumed to be inextensible but flexible, as opposed to stretchable. A model for the actuator is presented and validated with experimental results, showing capabilities of high strain, pushing and pulling, and independent control of length and stiffness. These characteristics are motivated by the application of a compliant truss robot. Accordingly, we show a simple grounded tetrahedron with three actuator elements and three static elements. We demonstrate motion of the tetrahedron apex against external loads and the ability of the structure to vary its stiffness. The actuator offers a unique set of characteristics that could increase the capabilities of soft robotic devices.

I. INTRODUCTION

Pneumatic artificial muscles (PAMs) are a popular form of actuation in robotics, especially with the recent increase in interest in soft robotics [1,2]. PAMs exploit the energy stored in compressed air to move, and offer axial stresses close to natural muscle, inherent compliance, high force to weight ratios, and high speeds, with the caveat that a pressure source is required [3]. One of the most attractive features of PAMs is the ability to create specialized characteristics by carefully designing the geometry of the actuator for a given application. For this work, the motivating application is the development of a truss robot, as shown in Fig. 1. There has been substantial research on creating robots made of a large number of linear actuators, connected into a mesh or truss type structure [4]-[7]. Such a robot could change its shape for locomotion, manipulation of objects, and interaction with its surroundings.

To expand the capabilities of truss robots, we aim to make an inherently compliant version, with PAMs acting as the truss elements. This application establishes three actuator requirements (in addition to inherent compliance): (1) a high extension ratio, (2) the ability to apply forces in both compression and tension, and (3) actuators that can independently vary their length and stiffness. While many existing actuators satisfy some of these requirements, we are unaware of a single device that satisfies them all. It is worth noting that the most popular PAM, the McKibben actuator, which is composed of flexible rubber tubing inside of a braided

This work was supported in part by National Science Foundation Grant 1196335 and US Army Medical Research and Materiel Command grant W81XWH-15-C-0091.

email: usevitch@stanford.edu, aokamura@stanford.edu, ewhawkes@engineering.ucsb.edu

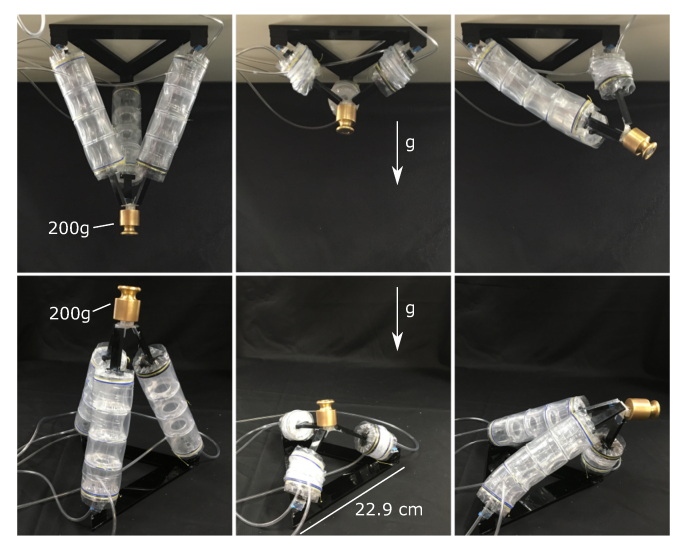


Fig. 1: A structure made of 3 APAM actuators. Each actuator is able to undergo large shape change, and support loads in both tension and compression.

sheath, while compliant, satisfies none of our additional requirements: it contracts by less than 30%, applies only tension, and has a stiffness that is correlated to length [8]–[10].

1) High Elongation Actuators: Many actuators have been designed that attempt to maximize the overall extension ratio of the device. While some of these actuators are made of rigid components, such as the Zippermast [11], there are also examples in the realm of inherently compliant PAMs. The inverse pneumatic artificial muscle (IPAM) is a radial constrained elastic tube capable of strain rates up to 300%, but is only able to reliably exert contractile forces [12]. The pneumatic reel actuator (PRA) uses inextensible material and applies moderate forces in two directions with extremely high extension ratios, but requires some mechanical complexity in the reeling mechanism [13]. Like many PAMs, the IPAM and the PRA also show a coupling between length and stiffness. For these actuators, the shorter their length, the lower their axial stiffness.

2) Push-Pull Actuators: Most PAMs, like the McK-ibben, are designed to pull, and are unable to apply large forces to push [8]. Less common are actuators designed to push, for example an origami-based PAM [14]. At least one PAM is designed to apply controlled pneumatic forces in both directions [15]. This actuator relies on 3 chambers, two that pull and one that pushes. However, use of the actuator for high elongation and the independent control of length and stiffness were not discussed. A simple bellows [16] could also act as a push-pull actuator if vacuum were applied to retract it, and the rings of bellows could maintain their

¹Department of Mechanical Engineering, Stanford University

²Department of Mechanical Engineering, University of California, Santa Barbara

Actuator Type	High	Push/Pull	Stiffness
	Elongation		Control
McKibben	No	No	No
Zippermast [11]	Yes	Yes	No
STIFF-FLOP [17]	No	Yes	Yes
Pneumatic Reel [13]	Yes	Yes	No
IPAM [12]	Yes	No	No
BiFAc3 [15]	No	Yes	No
Lead Screw	No	Yes	No

TABLE I: Comparison of general capabilities for a few linear actuators.

shape under vacuum. However, length and stiffness are not independently controllable in a bellows.

3) Independent Stiffness and Length Control: Finally, PAMs with independent control of stiffness and length are not common. One device controls its stiffness in a manner inspired by hydrostatic muscles found in nature, such as the octopus tentacle [17]. The device uses both pneumatic actuators as well as motor-driven pull-tendons to actively vary stiffness. Large strains were not a focus of the work. We summarize the comparison of our actuator with a few existing actuators in Table I.

In the current work, we present an Antagonistic Pneumatic Artificial Muscle, or APAM, that is capable of 1000% elongation, application of both pushing and pulling forces, and independent stiffness and length control. These characteristics are enabled by independently controlled concentric pressure chambers; each chamber can both push and pull in an antagonistic fashion. The chambers are made from thinwalled minimally extensible material that can completely collapse when the actuator is fully shortened. We begin with a description of the design, followed by presentation of an analytical model that relates actuator geometry and chamber pressures to length and stiffness. We briefly describe our fabrication methods. We then show results that verify our model and show the capabilities of APAMs. Finally, we demonstrate shape and stiffness changing in a tetrahedron with three of its six elements as active APAMs.

II. DESIGN

The APAM is made of two tubes of flexible but nearly inextensible material with one tube nested inside the other, so as to form an inner chamber (within the inner tube), and an outer chamber (between the inner and outer tube) that can be controlled to different pressures. Rings or disks are placed along the length of the tube to constrain the diameter of the inner tube to a constant value. A cross-section of one cell of the actuator at three different lengths is shown in Fig. 2. Multiple cells can be stacked to created longer actuators. If the length of the actuator (denoted L) is less than the membrane length L_o , and the pressure in the outer chamber is greater than the pressure in the inner chamber, the outer tube will wrinkle along the axial direction, while the diameter remains constant (pleats will form on planes perpendicular to the applied load). The inner tube will bulge inwards, creating the hourglass shape shown in Fig. 2, middle. This inner tube will wrinkle along the circumferential direction (pleats will form on planes parallel to the applied load).

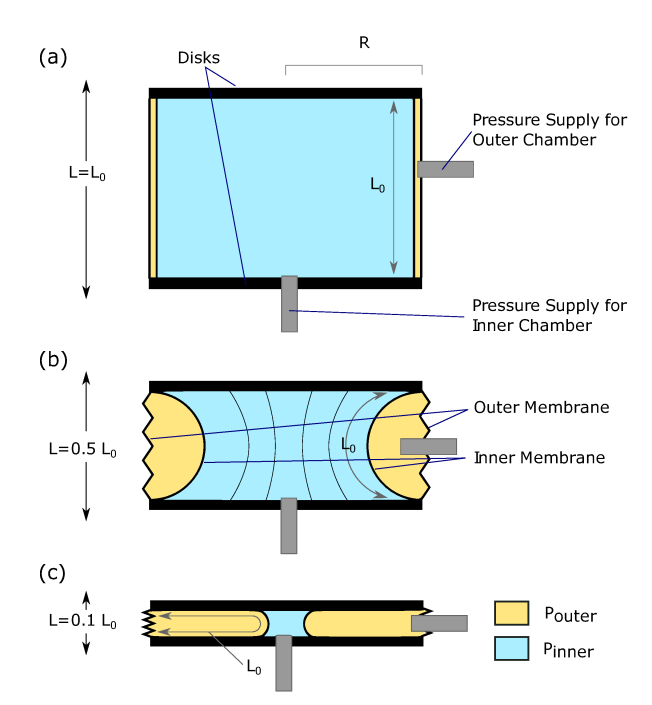


Fig. 2: Basic geometry of an APAM. A single cell is shown at three different levels of extension.

A. Working Principle

The movement of the actuator is driven by antagonistic forces caused by changing the pressure in the inner and outer chambers. The direction of the force applied by the inner chamber is simple: positive pressure in the inner chamber applies an extending force, while negative pressure applies a retracting force. The outer chamber is more complex; it applies either extending or retracting forces, depending on the length of the actuator. There is a length, L_{crit} , at which the volume in the outer chamber is at its maximum. If the length of the actuator is above L_{crit} , positive pressure in the outer chamber applies a retracting force. If the length of the actuator is below L_{crit} , positive pressure in the outer chamber applies an extending force.

Antagonistic action of the two chambers can be achieved at all lengths of the actuator. If $L < L_{crit}$, positive pressure applied to the outer chamber will tend to lengthen the APAM and vacuum applied to the inner chamber will tend to shorten it. These antagonistic forces can be tuned by the relative levels of the pressure and vacuum in the chambers. If $L > L_{crit}$, positive pressure applied to the outer chamber will tend to shorten the APAM and positive pressure applied to the inner chamber will tend to shorten it. This antagonistic action allows for control of the stiffness independent of length, and control of length independent of stiffness. The ability to apply vacuum to the inner chamber also enables extremely high extension ratios, as the volume of the inner actuator can be driven to nearly zero by removing air.

B. Device Geometry

The geometry of the device is defined by the number of cells included in series, the radius of the disks and tubing, R, and the rest length of the membranes between disks, L_0 .

The selection of L_0 and R must ensure that even in a fully collapsed state, the outer membranes from opposite side of the actuator do not meet in the middle and restrict airflow. The most contracted actuator at the bottom of Fig. 2 shows this situation: the inner membranes are almost touching in the center of the actuator. The constraint $L_0 < 2R$ ensures that airflow throughout the inner chamber is possible. We will limit our analysis to the case where $P_{outer} > P_{inner}$, otherwise the structure behaves as an inflated beam, as the volume of the outer chamber will be zero. We also assume that $P_{outer} > P_{atm}$, which ensures that the outer membrane always forms a cylinder of radius r. If $P_{outer} < P_{atm}$, the outer membrane will bulge inwards.

III. MODELING

We develop a model of the actuator by first relating the changes in pressures and volumes of the inner and outer chambers through the principal of virtual work. To determine the change in volumes, we analyze the membrane shape, and then use the assumed membrane shape to analyze the length and stiffness of an actuator with known pressure inputs.

A. Virtual Work

We use the principle of virtual work to determine the force and displacement relationships for the actuator. To do so, we imagine an infinitesimal axial displacement of the actuator, and equate to zero the sum of the work done by an applied axial load and the work done by the inner and outer pressure chambers

$$FdL + P_{inner}dV_{inner} + P_{outer}dV_{outer} = 0. (1)$$

$$F = -P_{inner} \frac{dV_{inner}}{dL} - P_{outer} \frac{dV_{outer}}{dL}$$
 (2)

In the case of this actuator, where the combined inner and outer chambers always form a cylinder, $V_{inner}=\pi R^2L-V_{outer}$. Thus, we can write

$$\frac{dV_{inner}}{dL} = \pi R^2 - \frac{dV_{outer}}{dL} \tag{3}$$

$$F = -P_{inner}\pi R^2 + (P_{inner} - P_{outer})\frac{dV_{outer}}{dL}$$
 (4)

This expression shows that for a fixed length and applied outer force, the relationship between P_{inner} and P_{outer} is linear, meaning that a constant length can be maintained as pressures are changing in a linear relationship.

We can take the derivative of Eq. 4 with respect to length to obtain an expression for the stiffness.

$$\frac{\partial F}{\partial L} = (P_{inner} - P_{outer}) \frac{d^2 V_{outer}}{dL^2} \tag{5}$$

This analysis has shown that it is possible to achieve the same lengths with different pressures, and that increasing the difference between the inner and outer pressure increases the stiffness. Next we compute $\frac{dV_{outer}}{dL}$ and $\frac{d^2V_{outer}}{dL^2}$, which requires identification of the membrane shape.

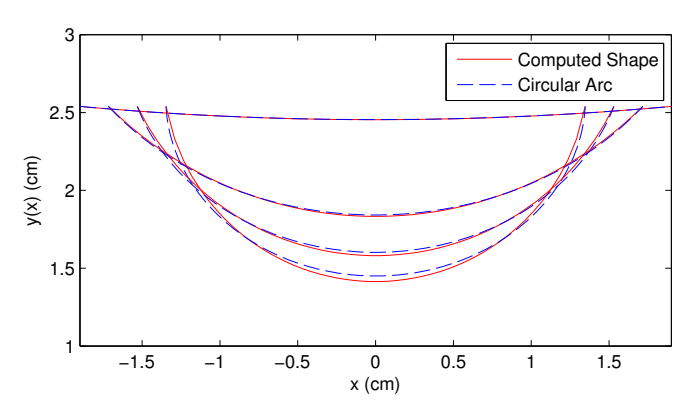


Fig. 3: The shapes of the membrane that minimize the internal volume (the solution to the boundary value problem), compared to circular arc of length L_0 =3.81 and R=2.54 with the same end conditions. Each pair of curves represents the solutions for different lengths of the actuator.

B. Membrane Shape

To compute the enclosed volume of the inner and outer chambers, we must first determine the membrane shape. If $P_{outer} > P_{inner}$, then the membrane will take a shape that maximizes the volume of the outer chamber, and minimizes the volume of the inner chamber. Assuming that the material is inextensible and the actuator is axi-symmetric, the problem becomes one of finding a curve of fixed length that satisfies the boundary conditions imposed by the actuator geometry and minimizes the volume enclosed when the curve is revolved about the center axis (minimizing the volume of the inner chamber and maximizing the volume in the external chamber). A 2D representation of the problem can be seen in Fig. 2(b). Using a calculus of variations approach from [8], finding such a curve y(x) is equivalent to solving the boundary value problem:

$$y''(x) = \frac{2\pi y(x)(1+y'(x)^2)^{3/2}}{\lambda}$$

$$y'(0) = 0, \quad y\left(\frac{L}{2}\right) = R$$

$$\int_0^{L/2} \sqrt{1+y'(x)^2} dx = \frac{L_0}{2}$$
(6)

where λ is an unknown parameter. While in [8] this expression is used to compute the maximum volume curve, the expression is for any extremal curve, meaning a curve that either maximizes or minimizes volume. Whether the solver converges to the maximal or minimal volume solution will depend largely on the initial condition. To solve this problem numerically, we define a new state, $v(y) = \sqrt{1 + y(x)^2}$, with the accompanying boundary conditions v(0) = 0, $v(\frac{L}{2}) = \frac{L_0}{2}$. This results in a third-order boundary value problem with one unknown parameter, λ , and 4 boundary conditions. We solve this problem numerically using Matlab's BVP4C solver. This numerical solving technique is sensitive to initial condition, so the initial guess of the system was given as the circular arc with positive concavity of length L_0 that satisfies the boundary conditions. We compare the resulting membrane shape to the circular arc used as an initial guess in Fig. 3. For this case of L_0 =3.81 cm and R=2.54 cm,

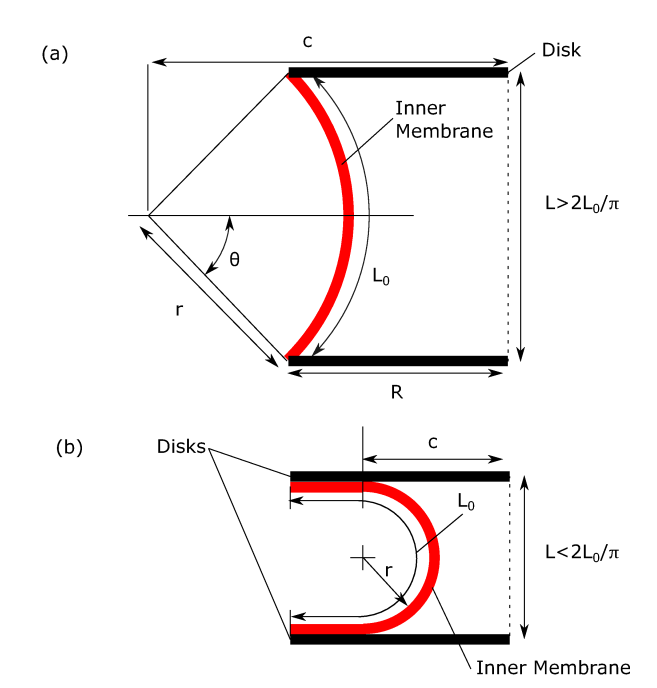


Fig. 4: The shape of the membrane and the parameters that define its definition in the case where the membrane is not in contact with the disks (a), and when the membrane is in contact with the disks (b). The membrane is shown in red.

the biggest difference in the resulting revolved volumes was less than 0.3%. Because the computed membrane shape does not differ significantly from the shape of the circular arc, our model will assume that the membrane takes the shape of a circular arc.

This circular arc model predicts that when $L < \frac{2L_0}{\pi}$, the center of the circular arc will be less than R, and the resultant arc will extend through the disks. In this case, we assume that the effective length of the membrane is shorter, and the extra membrane material contacts and lays flat along the disk. The membrane not in contact with the disk is in the shape of an arc that is a half circle. These two different cases and the geometry parameters that define them are shown in Fig. 4.

C. Rest Length Computation

Using the assumption that the membrane takes the shape of a circular arc, it is possible to compute the volume of the inner and outer chambers.

The volume of the inner chamber is given as

$$V_{\text{inner}} = 2 \int_0^{\frac{L}{2}} \pi y(x)^2 dx = 2 \int_0^{\frac{L}{2}} \pi (-\sqrt{r^2 - x^2} + c)^2 dx$$

where r is the radius of the circular arc and c is the center of the circle.

For the region where $L < \frac{2L_0}{\pi}$, meaning that the membrane is partially constrained along the rigid disks, $r = \frac{L}{2}$ and $c=R-\frac{1}{2}(L_0-\frac{L\pi}{2})$. This allows us to compute V_{outer} .

$$V_{outer} = -\frac{\pi}{24}L(6L_0^2 - 3\pi L_0 L - 24RL_0 + 4L^2 + 6\pi RL)$$
 (8)

We can then take the derivative with respect to L.

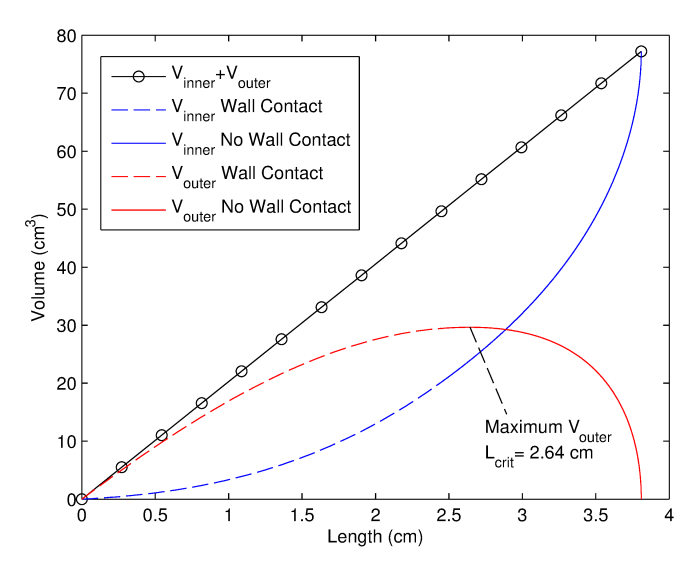


Fig. 5: The change in volume of the inner and outer chambers as the actuator changes length, for an actuator where $R=2.54~\mathrm{cm}$ and $L_0=3.81~\mathrm{cm}$. The maximum volume in the outer chamber occurs when L=2.64 cm. For all L < 2.43 (when contact between the inner membrane and the discs occurs), the geometry used in Fig. 4(b) is used to compute volume, while for L > 2.43, volume is computed using the geometry in Fig. 4(a).

$$\frac{dV_{outer}}{dL} = \frac{\pi}{4}(-2L^2 + (L_0 - 2R)\pi L + 4RL_0 - L_0^2)$$
 (9)

For the case where $L>\frac{2L_0}{\pi}$, we can define the following relationships from the geometry illustrated in Fig. 4.

$$L_0 = 2\theta r \tag{10}$$

$$\frac{L}{2} = r \sin \theta \tag{11}$$

$$L = L_0 \frac{\sin \theta}{\theta} \tag{12}$$

$$L = L_0 \frac{\sin \theta}{\theta} \tag{12}$$

These relationships allow us to solve for θ when given a length, which can be used to compute $r = \frac{L_0}{2\theta}$ and c.

$$c = R + \sqrt{r^2 - \left(\frac{L}{2}\right)^2} \tag{13}$$

We can then compute V_{outer} , and $\frac{dV_{\text{outer}}}{dL}$ as follows,

$$\frac{dV_{outer}}{dL} = \frac{\frac{dV_{outer}}{d\theta}}{\frac{dL}{d\theta}},\tag{14}$$

where

$$\frac{dL}{d\theta} = \frac{L_0}{\theta^2} (\theta \cos(\theta) - \sin(\theta)). \tag{15}$$

We computed $\frac{dV_{outer}}{d\theta}$ using Matlab's symbolic toolbox, and an analytic expression was found, but is not included here for brevity.

The changes in V_{inner} and V_{outer} with length are shown in Fig. 5. The volume of the outer chamber initially increases with increasing length, but obtains a maximum, and then decreases to 0 as the actuator reaches its maximum length.

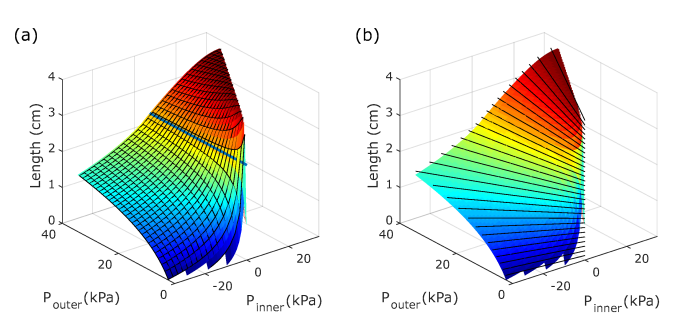


Fig. 6: The rest length of the actuator with no external load. (a) Constant pressure contours. (b) Constant length contours, which are linear in the pressures.

We denote the length at which the outer chamber achieves its maximum volume as L_{crit} .

The rest length of the actuator can be found by finding the length L where the output force is equal to zero. A plot of the input pressures and zero load length are shown in Fig. 6. In Fig. 6a, a blue trace marks the point where $L=L_{crit}$. If the actuator is above this length, then the increasing pressure in the outer membrane causes the actuator to shorten. If below this length, increasing outer pressure causes the actuator to lengthen. This means that depending on the length of the actuator, the outer chamber can switch between applying a pushing or a pulling force. In Fig. 6(b), the constant length contours on the plot are linear in the outer and inner pressures.

D. Stiffness

The dual inputs to this actuator allow direct control of the axial stiffness. The stiffness when $L < \frac{2L_0}{\pi}$ is $(P_{inner} - P_{outer}) \frac{d^2 V_{outer}}{dL^2}$, where $\frac{d^2 V_{outer}}{dL^2}$ is computed as the derivative of Eq. 9,

$$\frac{d^2V_{outer}}{dL^2} = \frac{\pi}{4}(\pi L_0 - 4L - 2\pi R). \tag{16}$$

This means that for the lower region of the stroke, stiffness varies linearly with height with constant pressure inputs.

For the region where $L > \frac{2L_0}{\pi}$, we can write

$$\frac{d^2V}{dL^2} = \frac{\frac{d}{d\theta} \left(\frac{dV_{outer}}{dL}\right)}{\frac{dL}{d\theta}}.$$
 (17)

This derivative was computed using Matlab's symbolic toolbox, and can be found analytically, but is not presented here for brevity.

We use these results to generate Fig. 7, which relates length, stiffness, and P_{inner} and P_{outer} . This plot shows changes in length and stiffness with contours of constant inner and outer pressure. This plot also gives a user the ability to quantify what lengths and stiffnesses are achievable for given pressure limits.

IV. FABRICATION

In this section we will present various instantiations of APAMs that differ in the materials used and construction. In all versions, the key mechanical requirement that must be enforced is that the inner membrane stays constrained to

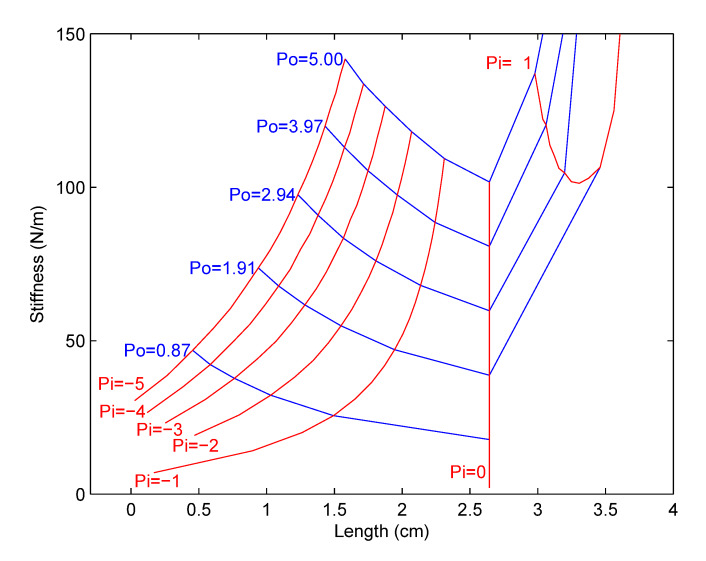


Fig. 7: The changes of stiffness and zero load length with constant pressure contours. This plot also gives information on the stiffness and length change that are possible given pressure limits imposed by the actuator materials.

the actuator's outer radius at the boundary of each cell. We achieve this requirement in two ways. In the first method, we place disks on the inside of the inner tube. In the second method, we attach the inner membrane to the outer membrane, and then constrain the outer membrane with external rings.

All of the components and a completed actuator are shown in Fig. 8. The membrane of the actuator is low-density polyethylene (LDPE) lay-flat tubing, 0.04 mm thick. The disks are a sandwich of three layers of 1.6 mm thick laser-cut acrylic with the center and three notches removed. The center piece of the sandwich has a 22 mm diameter, while the outer two pieces have a 25 mm diameter. This forms a groove around the perimeter of the disk. The disks are inserted inside the inner membrane, and then a string is looped around the outer membrane, and tightened until it fits into the assembled disks circumferential groove. The central hole in the disks allows air to flow through the inner chamber, and the notches around their perimeter allows air to flow through the outer chamber. For further details on fabrication, refer to the attached video.

The maximum pressure that can be applied to the LDPE tubing is limited by the material strength, and the material degrades after hundreds of cycles. As another option, we assembled devices out of silicone-impregnated reinforced nylon. For this material, the tubing was made by rolling a sheet of the nylon fabric and adhering the material to itself at the proper diameter using SmoothOn Sil-poxy silicone adhesive. Disks were inserted using the string method described above.

As a minor practical consideration, the reinforced nylon fabric is opaque while the LDPE tubing is not. Most of the actuators we show in this paper are made from LDPE because their transparent nature enables easier visualization of the behavior of the inner chambers. We use a reinforced nylon actuator to characterize the device because it enables higher pressure levels, and is more robust to puncture, and

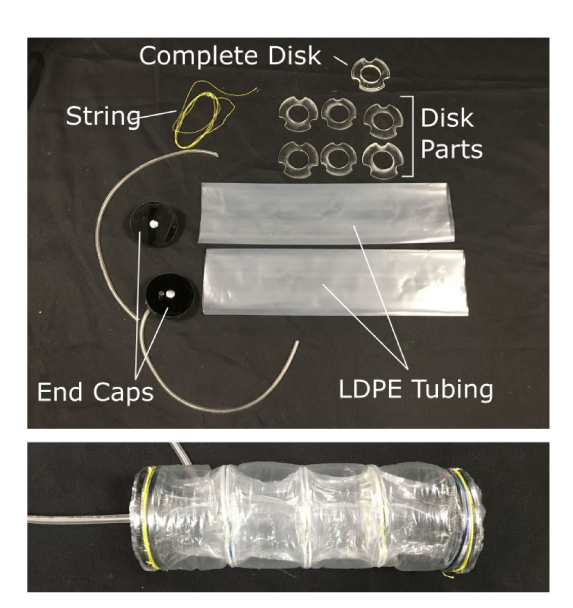


Fig. 8: All of the components used to fabricate one 4 cell actuator and a completed actuator.

provides more repeatable results because the material does not degrade.

We input or remove air from the inner chamber by passing a tube through one of the actuator end caps. We insert an additional tube through the side wall of the outer membrane to supply the outer chamber with pressure.

V. RESULTS

A. Single Cell Test Setup

To understand the load displacement properties of the APAM, the test setup shown in Fig. 9 was developed to test a single rip-stop nylon APAM cell. The tested actuator used $R=2.54~\rm cm$ and $L_o=3.81~\rm cm$. The setup consists of a manually controlled linear stage, and a Mark-10 Force Gauge Series 4. Data was gathered by setting the desired pressures in the inner and outer chamber using mechanical pressure regulators (IMI Norgren R07-200-RNEA), beginning at the shortest length of the actuator and increasing the length in increments of 0.254 cm. We took a static measurement of force at each length until the maximum height was reached, and then decreased the length to the minimum by same increments, again measuring the force at each length.

B. Load Displacement Curves

The gathered data from the single cell load test is compared with the force and length model developed in Section III, with the results displayed in Fig. 10. In Fig. 10(a), the outer pressure is maintained at a constant 14 kPa while the inner pressure is varied from -20 kPa to 10.3 kPa. Fig. 10(b) shows the resulting force displacement curves when the inner pressure is maintained at 0 kPa and the outer pressure is varied from 6.9 kPa to 13.7 kPa. The model seems to capture the trend and magnitude of the data. We compute the the error as the absolute value of the difference between the predicted and measured force of the actuator at a given length. When the actuator is shorter that 3.25 cm, the average error was 1.4 N, with a maximum error of 7.5 N. At lengths, greater than 3.25 cm accuracy decreases as the theoretical

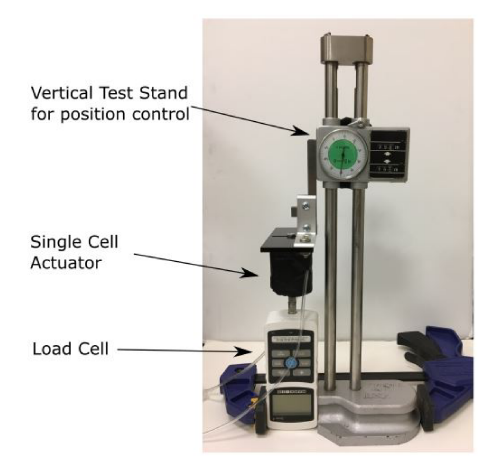
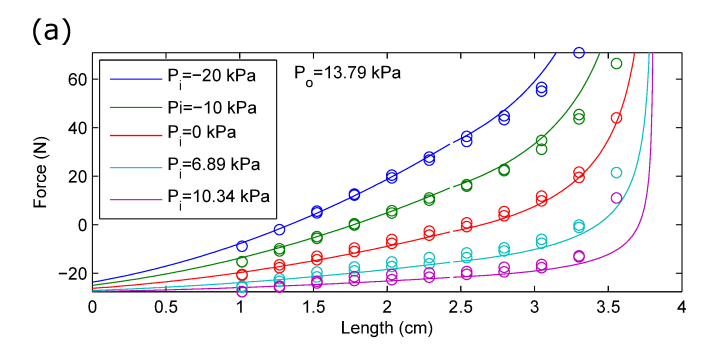


Fig. 9: The setup used to obtain force/displacement data for the actuator. Data was collected using a single cell actuator fabricated from rip-stop nylon, which provide more repeatable results than LDPE actuators.



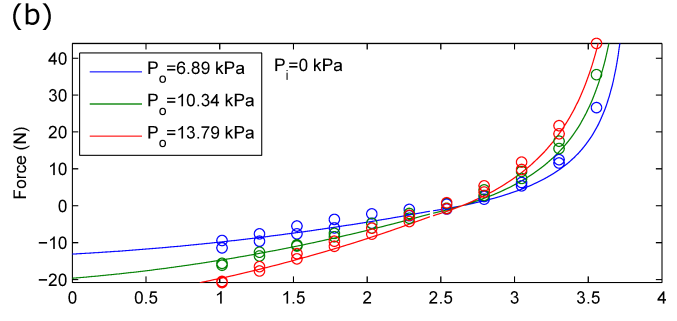


Fig. 10: Comparison of the APAM model with experimental data gathered from the single cell test mechanism. (a) Change in load displacement curve with increasing inner pressure. (b) Change in load displacement characteristics with changing outer pressure. The solid lines are the model predictions, and the points are the measurements.

load approaches infinity. In all cases, the actuator can exert large tension force when $L=L_0$, as in this case all load is carried by the undeformed membrane. The general effect of increasing the internal pressure is to lower the slope of the curve and push it downwards. In contrast, increasing the outer pressure makes the curve steeper. In Fig. 10(b), the three curves cross at a point. For this particular case of no inner pressure, this length is the zero load length of the actuator, and corresponds to the configuration that maximizes the volume of the outer chamber. At that length, slope of the force deflection curve, and hence the stiffness, can be changed by changing the pressure in the outer chamber without affecting free length.

The maximum forces and stiffness that can be achieved by this actuator are primarily limited by the pressures that

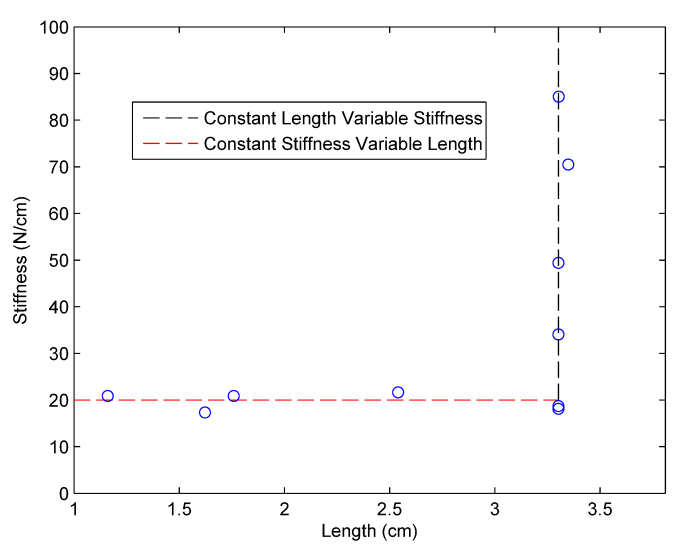


Fig. 11: Data showing various measured length-stiffness combinations of an APAM. A stiffness of roughly 20 N/cm can be maintained while increasing length, and a length of roughly 3.3 cm can be maintained while increasing stiffness.

the material can withstand. For the single cell prototype of reinforced nylon, a pressure of about 50 kPa caused the connection between the nylon and the endcaps to fail. The LDPE tubing used in other prototypes throughout this paper begins to plastically deform when the outer chamber is at a pressure of 20 kPa. Improved materials and manufacturing could allow higher pressure and larger output forces.

C. Independent Length and Stiffness Change

From each of the force-displacement curves we obtained, we used linear interpolation to extract the point of zero force and approximate the slope of the force-displacement curve at that point. This gives us the no-load length and stiffness for a given pressure combination. We plot several of these points to show that independent change of length and stiffness is possible (Fig. 11).

D. Maximum Strain

An APAM was tested to measure the maximum attainable strain. The shortest length, measured at 9 mm, is achieved with no pressure in the outer chamber and vacuum in the inner chamber. The longest state is positive pressure only in the inner chamber and its length was measured at 130 mm. Maximum strain calculated as 1400% (Fig. 12). The extension ratio is primarily limited by the thickness of the disks and the collapsed membrane. The version tested has thin fiberglass discs with 0.025 mm thickness and LDPE membrane with 0.015 mm thickness.

E. Grounded Tetrahedron Robot

To show the capabilities of the actuator in a robotic truss system, the motivating application of this work, we constructed a portion of a tetrahedron robot, consisting of three actuators attached to a triangular base, as shown in Fig. 1. Each actuator is composed of 4 different cells.

This tetrahedron robot was constructed by attaching three actuators to the vertices of the base with a single 1-DOF nylon hinge (from Du-Bro). At the center point, each actuator

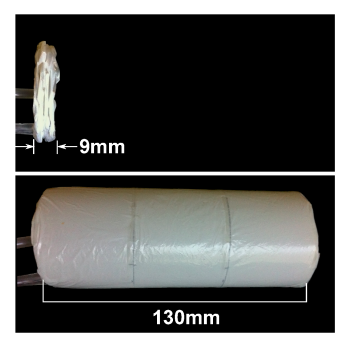


Fig. 12: Maximum strain of an APAM was measured at approximately 1400%.

was attached to another hinge, and the three hinges were bolted together. This means that if the actuators were unable to bend or twist, the device would have only one degree of freedom, with the center point moving perpendicular to the base plane. However, the natural compliance of the actuators allows the device to obtain other configurations.

To show that the actuators were able to support loads in both tension and compression while moving through sizable displacements, a 200 g mass was attached to the center point, and the robot was maneuvered to various configurations. This was repeated for both the upright and inverted case, as shown in Fig. 1.

To demonstrate the ability of the robot to change stiffness while maintaining length, the top row of Fig. 13 shows two configurations with different stiffnesses but similar configurations. When placed under a 7.5 N load, the stiffer device deforms slightly, but the more compliant truss collapses.

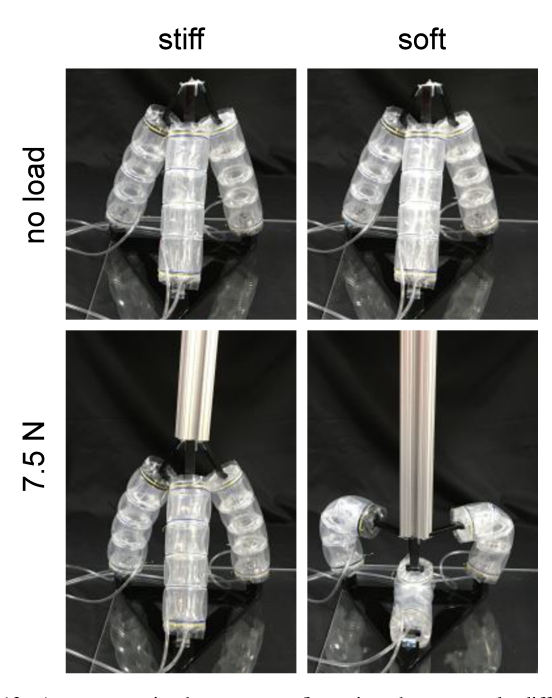


Fig. 13: An actuator in the same configuration that responds differently to applied loads. *Top:* With no applied load, the actuators look identical. *Bottom:* Under applied load, the tetrahedron with the stiffer actuators supports the load with some deflection (left), while the less stiff robot collapses (right).





Fig. 14: Demonstration of a length-controlled bending device where the outer chamber is separated into three chambers that run the length of the device. One of these three outer chambers is pressurized. On the left, the pressure in the inner chamber is positive, while on the right the pressure in the inner chamber is negative. When the device is long, the pressurized outer chamber exerts a contractile force; when the device is short, the inflated outer chamber exerts a pushing force, reversing the curvature.

F. Soft Bending Device

As a variation on this actuator design, we created a device where the outer chamber is divided into three separate chambers that run the length of the actuator. Actuation of these individual cavities applies asymmetric forces to the actuator, which cause it to bend. An interesting behavior occurs if one outer cavity is inflated, and the inner cavity is changed from positive pressure to negative pressure. When the inner chamber is at a positive pressure, $L > L_{crit}$, and the pressure in the one outer chamber exerts an contracting force on the device. This results in bending toward the one inflated outer chamber. When vacuum is applied to the inner chamber, $L < L_{crit}$, and the one outer chamber exerts an extending force, switching the direction of the curvature. This demonstrates that pressure in the outer chamber can lead to either pushing or pulling forces, depending on actuator length.

VI. CONCLUSION

The APAM has the ability to independently control stiffness and length over a large extension range while either pushing or pulling, making this actuator valuable for a variety of applications. One target application is the construction of robots made up of a large number of linear actuators connected into a network. The large extension ratio of this actuator, as well as its ability to control stiffness independently of length, would greatly increase the capabilities of truss robots. A computational model is presented that relates how the pressure inputs correspond to rest length and stiffness. We have demonstrated this actuator in a grounded tetrahedron robot, and as a soft bending device. One limitation of this approach is that, like all all pneumatic devices, a pressure source is required, meaning that a mobile robot will be required to carry either a pump, a compressed air cartridge, or some other source of pressure. The APAM also requires vacuum, which can be delivered either through a pump or a Venturi mechanism. Another consideration is that the APAM is not completely soft. This is the case for many soft robots, and must be taken into account when designing for specific applications. Versions using compliant superelastic

Nitinol wire formed into loops as replacements for the acrylic discs could allow for a more robust and fully flexible APAM. Future work will analyze the bending and buckling stiffnesses of the APAM, as well as integrate these actuators into mobile compliant truss robots.

REFERENCES

- [1] D. Rus and M. T. Tolley, "Design, fabrication and control of soft robots," *Nature*, vol. 521, pp. 467–475, 2015.
- [2] C. Laschi, B. Mazzolai, and M. Cianchetti, "Soft robotics: Technologies and systems pushing the boundaries of robot abilities," *Science Robotics*, vol. 1, no. 1, p. eaah3690, 2016.
- [3] I. W. Hunter, J. M. Hollerbach, and J. Ballantyne, "A comparative analysis of actuator technologies for robotics," *Robotics Review*, vol. 2, pp. 299–342, 1991.
- [4] S. Curtis, M. Brandt, G. Bowers, G. Brown, C. Cheung, C. Cooperider, M. Desch, N. Desch, J. Dorband, K. Gregory et al., "Tetrahedral robotics for space exploration," *IEEE Aerospace and Electronic Sys*tems Magazine, vol. 22, no. 6, pp. 22–30, 2007.
- [5] A. Spinos and M. Yim, "Towards a variable topology truss for shoring," *IEEE Ubiquitous Robots and Ambient Intelligence*, pp. 244– 249, 2017.
- [6] G. J. Hamlin and A. C. Sanderson, "Tetrobot: A modular approach to parallel robotics," *IEEE Robotics & Automation Magazine*, vol. 4, no. 1, pp. 42–50, 1997.
- [7] N. Usevitch, Z. Hammond, S. Follmer, and M. Schwager, "Linear actuator robots: Differential kinematics, controllability, and algorithms for locomotion and shape morphing," *IEEE International Conference* on Intelligent Robots, pp. 5361–5367, 2017.
- [8] F. Daerden and D. Lefeber, "Pneumatic artificial muscles: actuators for robotics and automation," *European Journal of Mechanical and Environmental Engineering*, vol. 47, no. 1, pp. 11–21, 2002.
- [9] C.-P. Chou and B. Hannaford, "Measurement and modeling of Mckibben pneumatic artificial muscles," *IEEE Transactions on Robotics* and Automation, vol. 12, no. 1, pp. 90–102, 1996.
- [10] B. Tondu and P. Lopez, "Modeling and control of Mckibben artificial muscle robot actuators," *IEEE Control Systems*, vol. 20, no. 2, pp. 15–38, 2000.
- [11] F. Collins and M. Yim, "Design of a spherical robot arm with the spiral zipper prismatic joint," *IEEE International Conference on Robotics* and Automation, pp. 2137–2143, 2016.
- [12] E. W. Hawkes, D. L. Christensen, and A. M. Okamura, "Design and implementation of a 300% strain soft artificial muscle," *IEEE International Conference on Robotics and Automation*, pp. 4022–4029, 2016
- [13] Z. Hammond, N. Usevitch, E. Hawkes, and S. Follmer, "Pneumatic reel actuator: Design, modeling, and implementation," *IEEE Interna*tional Conference on Robotics and Automation, pp. 883–888, 2017.
- [14] R. V. Martinez, C. R. Fish, X. Chen, and G. M. Whitesides, "Elastomeric origami: Programmable paper-elastomer composites as pneumatic actuators," *Advanced Functional Materials*, vol. 22, no. 7, pp. 1376–1384, 2012.
- [15] C. Ferraresi, W. Franco, and G. Quaglia, "A novel bi-directional deformable fluid actuator," *Proceedings of the Institution of Mechanical Engineers, Part C: Journal of Mechanical Engineering Science*, vol. 228, no. 15, pp. 2799–2809, 2014.
- [16] S. Kawamura and Y. Hayakawa, "A new type of pneumatic robot using bellows actuators with force sensing ability," in *IEEE International Conference on Robotics and Automation*, 1994, pp. 2451–2456.
- [17] A. Shiva, A. Stilli, Y. Noh, A. Faragasso, I. De Falco, G. Gerboni, M. Cianchetti, A. Menciassi, K. Althoefer, and H. A. Wurdemann, "Tendon-based stiffening for a pneumatically actuated soft manipulator," *IEEE Robotics and Automation Letters*, vol. 1, no. 2, pp. 632–637, 2016